Supplemental Figure Legends:

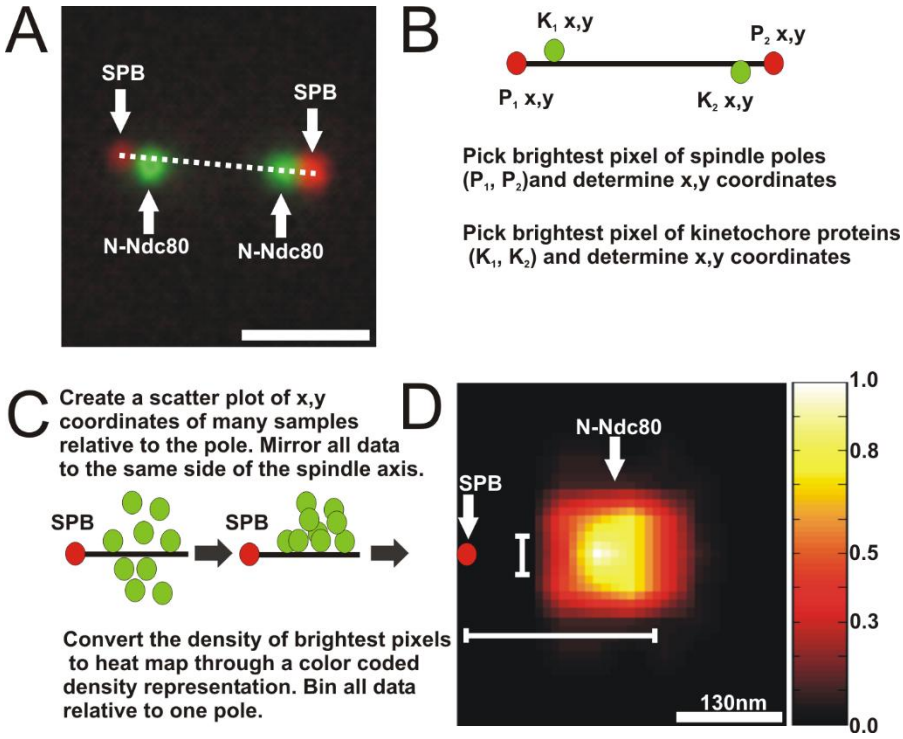

Figure S1 Related to Fig. 1, 2. Method to generate probability maps of kinetochore proteins (Ndc80-GFP) to visualize the three-dimensional arrangement of the kinetochore in metaphase and anaphase. The average position of Ndc80 was determined in metaphase and anaphase spindles in vivo.

A. Metaphase spindles are shown top left. Spindle pole bodies (Spc29-RFP) are in red, and kinetochores (N-Ndc80-GFP) are in green. The peak intensity (brightest pixel) of each focus was determined and the coordinates of each spot was plotted relative to the spindle pole body. Scale bar = 1uM

B., C. The number and position of Ndc80 foci were used to generate a positional density map representing the distribution of Ndc80 as a fraction of the distance (X) from the center of the spindle pole and position off the spindle axis. To generate the map we assume the poles are equivalent and orient both kinetochores to the same pole (indicated in C, See Experimental Procedures).

D. The distribution of the brightest pixels is shown using a color coded density map below, right with white and yellow the most likely and black and dark red the least likely (metaphase, n =1032). The black body radiation scale reduces artifacts due to the differential visual sensitivity to red, green, and blue color spectrum [1]. The position of Ndc80 in the half-spindle is shown. The horizontal bar (white) below the position of Ndc80 indicates the average distance along the x-axis from the spindle pole (SPB red spot). The vertical bar (white) left of Ndc80 indicates the average displacement along the y-axis. Scale bar = 130nm.

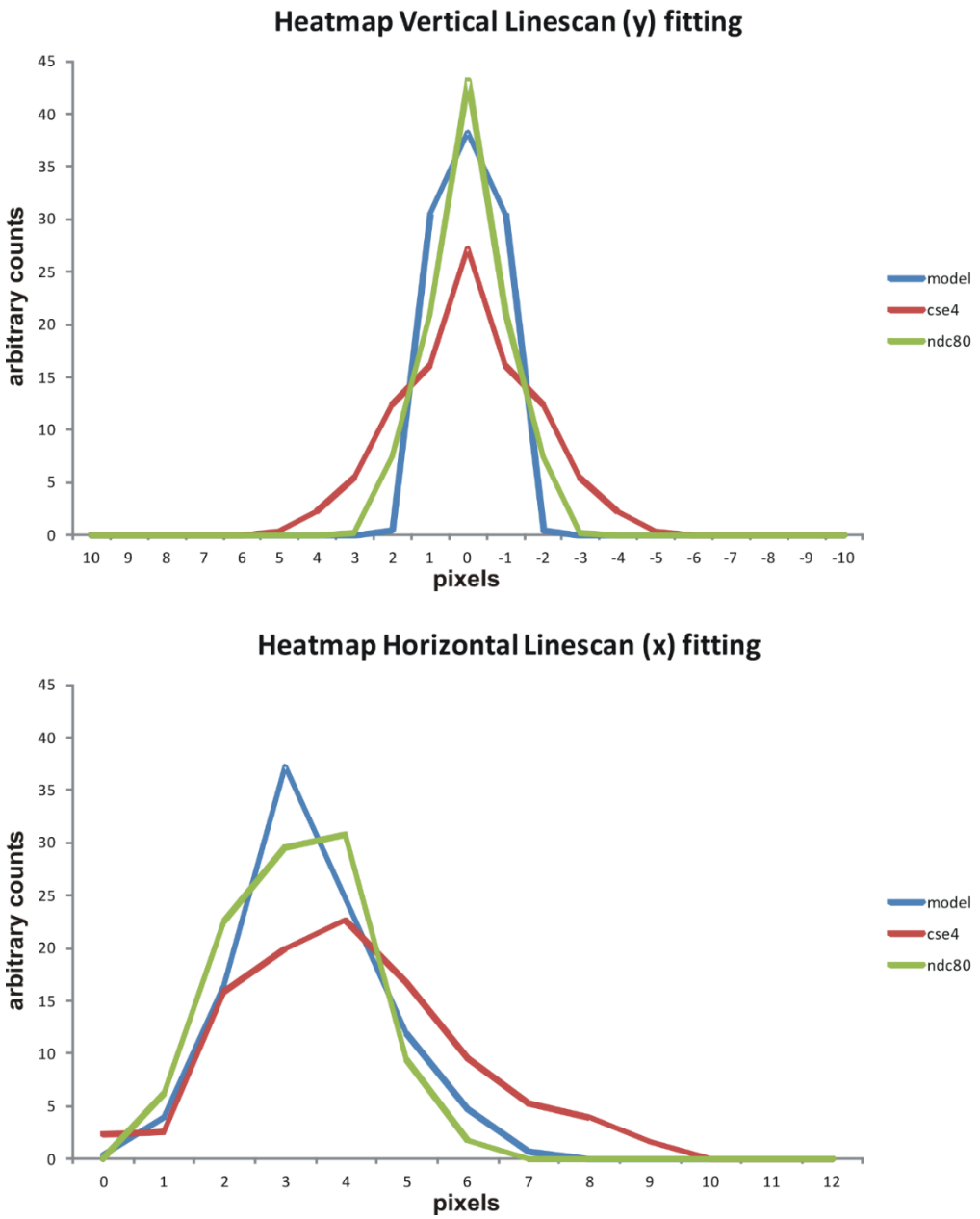

Fig. S2 related to Figure 2. Line scans of experimental vs. simulation density maps Experimental and simulated density maps were analyzed by line scans through the x- and y-axis. The simulation is built from populating the microtubule plus-ends in a mathematical model [2] (blue line). Line scans through experimental images for Ndc80 (green) and Cse4 (red) are shown. The scans of simulation and Ndc80 are similar, while the simulations do not faithfully reproduce the distribution of Cse4. Experimental images of Cse4 are much broader than the distribution of microtubule plus-ends. X-axis, pixels; y-axis, arbitrary units.

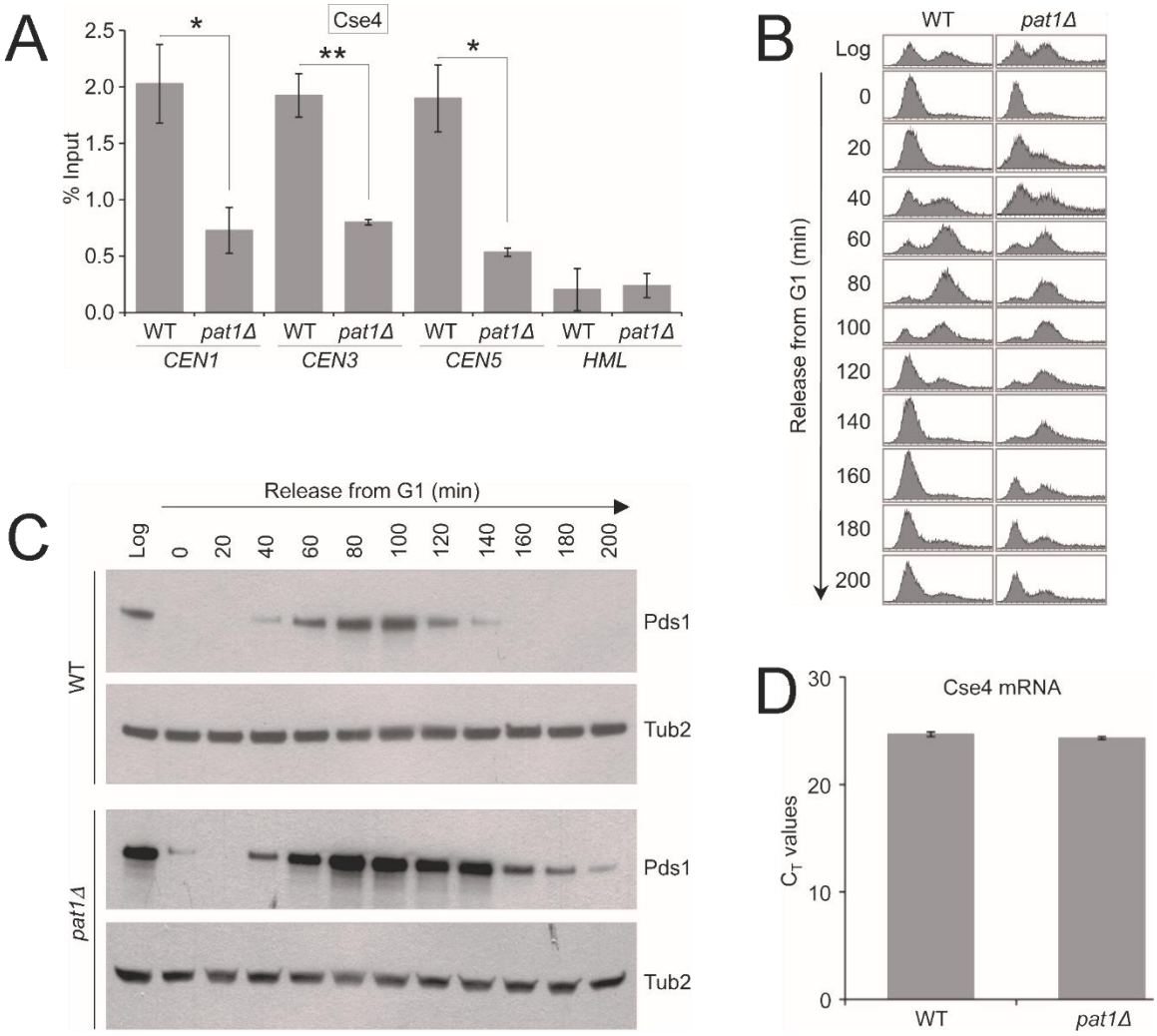

Fig. S3 related to Fig. 3B. (**A**) CEN association of Cse4 is reduced in *pat1Δ* strain. Centromeric levels of Cse4 were assayed by ChIP analysis of Cse4-Myc at CEN (CEN1, CEN3, and CEN5) and non-CEN (HML) DNA in wild type (WT, YMB6398) and *pat1*Δ (YMB8422) strains. Primary antibodies used were a-Myc (Z-5, sc-789, Santa Cruz Biotech). Enrichment was determined by qPCR and is shown as % input. Average from three biological experiments ± standard error is shown. *p value <0.05, **p value <0.01, Student's t test. (**B**) Pat1 is required for cell cycle progression. Deletion of *PAT1* (*pat1Δ)* results in delay in cell cycle progression. Wild-type (WT, YMB8713) and *pat1*Δ (YMB8714) strains with endogenously expressed Pds1-Myc were grown in YPD at 30°C, synchronized in G1 with α-factor, and released into pheromone-free YPD medium. Samples were taken at time points (min) after release from G1. DNA content was determined by FACS. (**C**) Degradation of anaphase inhibitor protein Pds1 is delayed in *pat1Δ* strains. Western blots showing protein levels of Pds1-Myc and Tub2 from strains described in (A). Primary antibodies used were a-Myc (Z-5, sc-789, Santa Cruz Biotech), a-Tub2 (Rabbit polyclonal antibodies against Tub2p were custom made by Covance, Inc.). (**D**) Transcription of the CSE4 gene is not affected in *pat1Δ* strain. Total RNA was extracted from wild type (WT, YMB6398) and *pat1⊿* (YMB8422) strains grown in YPD at 30°C. Level of *CSE4* transcripts was determined by real-time quantitative RT-PCR using 500 ng total RNA based on amplification of a 479 bp product using gene-specific primers. The C_T (cycle

threshold) values correspond to the number of PCR cycles needed to cross the threshold fluorescence in the amplification curve (t½ of the exponential region of amplification). CT is a relative measure of the concentration of Cse4 mRNA in the qRT-PCR reactions. Average C_T values from three independent biological experiments ± standard error are shown.

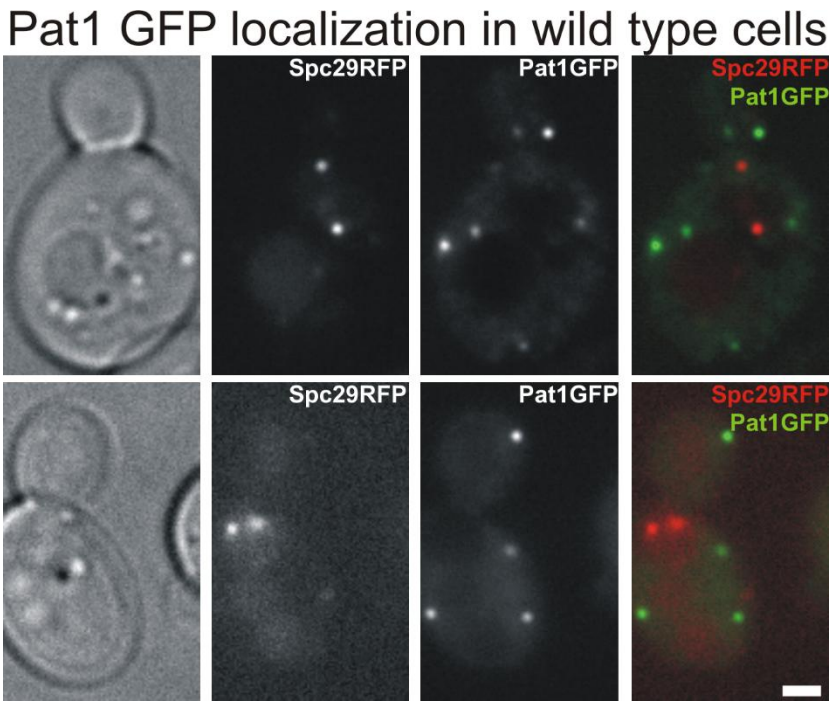

Fig. S4 related to Fig. 3B. Pat1-GFP localizes to cytoplasmic foci. Pat1-GFP imaging in wild type cells reveals multiple cytoplasmic foci. Left panel, cells visualized in DIC. Middle left, spindle poles visualized with the spindle pole marker Spc29-RFP.The cells are in mitosis as evidenced by a short (1-2micron) spindle near the neck of the budded cell. (middle right), Pat1-GFP cytoplasmic foci appear as diffraction limited spots throughout the mother and budded cell. (right panel) color overlay, Spc29-RFP in red, Pat1-GFP in green. There is no evidence for nuclear localization of the Pat1-GFP foci. Scale bar = 1uM

Supplemental Table 1:

Distance in X	X	X+10	X+20	X+30	X+40	X+50
Measured distance in X	237.06	247.89	256.18	268.92	279.76	286.13
st dev	45.41	44.56	35.22	55.67	56.97	57.31
width in Y	91.70	93.00	80.21	96.85	99.41	101.96
st dev	59.53	58.93	66.07	59.80	68.88	69.96
abs error in increase (from input change of 10)	n/a	10.83	8.28	12.75	10.83	6.37
average measured increase	9.81					
st dev	2.49					
average abs error in increase	1.95					
average st dev	49.19					

Table S1, related to Figure 1, 2. Model Convolution to assess localization accuracy of statistical probability maps.

Kinetochore microtubule lengths were determined from a mathematical model of the yeast spindle [2]. These measurements were mapped onto a three dimensional geometric representation of the spindle [3] based on experimentally derived EM and tomography measurements of kinetochore microtubules arranged in a 250 nm diameter cylindrical array. The model was populated with fluorophores and convolved to simulate an experimental image (model convolution [3, 4]). The kinetochore microtubule lengths were tuned to lie between Ndc80 (219nm) and Cse4 (286nm). We populated the microtubule plus-ends with fluorophores and determined the statistical probability map from hundreds of simulated images. From the statistical maps we determined the axial distance (x axis) and lateral spread (width in y). Microtubule lengths were manually lengthened in 10nm increments, up to 50nm. The axial distance and radial widths were determined for each 10nm increment. Each measurement represents a statistical map from > 200 images. The model and simulation-based density maps provide a quantitative approach to deduce the absolute position of kinetochore proteins from the experimental-based statistical maps.

Supplemental Table 2:

	Cse4	Ndc80
Brightest X	261.92 nm	201.20 nm
Gaussian X	261.96 nm	201.19 nm
Brightest Y	157.96 nm	158.27 nm
Gaussian Y	157.99 nm	158.27 nm
Average Error X	-2.88 nm	0.58 nm
Average Error Y	-2.19 nm	-0.15 nm

Table S2, related to Figure 1. Centroid vs. Brightest Pixel Accuracy

To assess the localization accuracy of the 2-dimensional density maps compared the statistical maps derived from centroids of Gaussian fits to the foci versus those derived from the brightest pixel method. Ndc80-GFP and Cse4-GFP foci were analyzed in metaphase. Spindles between 1.4-1.6 microns were used and aligned as described in Experimental Procedures. For centroid analysis, a Gaussian probability distribution was fit onto the foci. The center of the Gaussian was selected and used to create a statistical probability map. The brightest pixel method did not employ a probability distribution; rather the brightest pixel was selected and used to create a statistical probability map. The average position from both methods (along the spindle axis, x; and perpendicular to the spindle axis, y) are shown. The error in measurement between Ndc80 centroid of a Gaussian distribution vs. brightest pixel is less than 1nm, and for Cse4 centroid of a Gaussian distribution vs. brightest pixel to be between 2-3nm. The average error is less than a few nanometers. Thus the statistical maps for Ndc80 and Cse4 yield virtually identical results.

Supplemental Experimental Procedures:

Model Convolution:

For simulation, coordinates from the mathematical model [2] were mapped onto a three dimensional geometric representation of the spindle [3] based on experimentally derived EM and tomography measurements of kinetochore microtubules arranged in a 250 nm diameter cylindrical array [5]. Model parameters include spindle length (1.5 microns), spindle pole (250nm dia.), and dynamic kinetochore microtubules, average length of 230nm. The inner polar microtubules are surrounded by the shorter kinetochore microtubules. The model was populated with fluorophores and convolved to simulate an experimental image (model convolution [3, 4]). The mathematical model and geometric transfer accurately recapitulates key features of experimental data including spindle length and width, spindle length variation; kinetochore clustering and asymmetric chromatin stretching [6]. We then populated the microtubule plus-ends with fluorophores and determined the statistical probability map from hundreds of simulated images (Fig. 2, Model). The distribution along the spindle axis (x) of microtubule plus-ends in the model can be tuned to approximate the position of Ndc80 (Fig. 2 N-Ndc80). For simulated images, the mean axial position of the cluster of 16 microtubule plus-ends is 219± 49nm from the pole (Fig. 2 Model), while the mean radial position along the y-axis (radial direction) is 90 ± 80nm. These values are nearly identical to experimental values for Ndc80: the mean axial position is 219 ± 76nm and radial position is 94±94 nm. Thus the distance from the pole, as well as spatial organization (off-axis) and standard deviation for the simulated microtubule plus ends recapitulates experimental images of the Ndc80 microtubule binding kinetochore component. If there was significant variation of Ndc80 on individual microtubules, experimental images would fail to match simulation. Therefore Ndc80 molecules on a single microtubule are in register with one another.

RNA quantitation:

Wild-type (YMB6398) and *pat1Δ* (YMB8422) strains were grown in YPD at 30°C to logarithmic phase. Cells were collected by centrifugation and used for RNA extraction using RNeasy columns (Qiagen Inc., USA) following manufacturer's instructions. Real-time quantitative RT-PCR was performed to determine the levels of *CSE4* transcripts using 500 ng of total RNA and *CSE4* gene specific primers. Reactions were done in a 20-uL volume in a 7500 Fast system real-time thermocycler using *POWER* SYBR Green RNA to C_T 1-step Kit (Applied Biosystems, USA). Amplification conditions were as follows: 48°C for 30 min (RT step), 95°C for 10 min (enzyme inactivation), followed by 60 cycles of 95°C for 15 sec and 60°C for 1 min. Three independent biological replicates were performed.
Cse4 Primer Sequences:
OMB2153 AACAACAATGGGTTAGTTCTGC
OMB2154 TTTCACTAGCCTTGCAAATGG

Strains used in this study:

KBY8116 MATa trp1 Δ 63 leu2Δ ura3-52 his3 Δ 200 lys2-8 Δ1 NDC80GFP:KAN SPC29RFP:Hg

KBY8092 MATa trp1 Δ 63 leu2Δ ura3-52 his3 Δ 200 lys2-8 Δ1 Cyc1p-GFPNDC80:NAT (N terminal tag) SPC29RFP:Hg

MAY8543 MATa trp1 Δ 63 leu2Δ ura3-52 his3 Δ 200 lys2-8 Δ1 ASK1Cherry:KANMX SPC29CFP:Hg

KBY9075 MATa trp1 Δ 63 leu2Δ ura3-52 his3 Δ 200 lys2-8 Δ1 NUF2GFP:URA3 SPC29RFP:Hg

MAY8513 MATa trp1 Δ 63 leu2Δ ura3-52 his3 Δ 200 lys2-8 Δ1 SPC24CFP:KAN SPC29RFP:Hg

KBY6029 MATa trp1 Δ 63 leu2Δ ura3-52 his3 Δ 200 lys2-8 Δ1 CEP3GFP:HIS3 Spc29RFP:Hg

KBY2012 MATa trp1 Δ 63 leu2Δ ura3-52 his3 Δ 200 lys2-8 Δ1 CSE4GFP:TRP1 (pKK1) SPC29CFP:KAN

KBY 8166 MATa trp1 Δ 63 leu2Δ ura3-52 his3 Δ 200 lys2-8 Δ1 CSE4GFP:TRP1 (pKK1) SPC29CFP:KAN pat1Δ:NAT

KBY8168 MATa trp1 Δ 63 leu2Δ ura3-52 his3 Δ 200 lys2-8 Δ1 NDC80GFP:KAN Spc29RFP:Hg pat1Δ:Nat

YMB6398 *MATa ura3-52 lys2-801 ade2-101 trp1Δ63 his3Δ200 leu2Δ1 CSE4-13Myc::LEU2*

YMB8422 *MATa ura3-52 lys2-801 ade2-101 trp1Δ63 his3Δ200 leu2Δ1 CSE4-13Myc::LEU2 pat1Δ::URA3*

YMB8713 *MATa ura3-52 lys2-801 ade2-101 trp1Δ63 his3Δ200 leu2Δ1 PDS1-18Myc::LEU2*

YMB8714 *MATa ura3-52 lys2-801 ade2-101 trp1Δ63 his3Δ200 leu2Δ1 pat1Δ::URA3 PDS1-18Myc::LEU2*

YMB6398 *MATa ura3-52 lys2-801 ade2-101 trp1Δ63 his3Δ200 leu2Δ1 CSE4-13Myc::LEU2*

YMB8422 *MATa ura3-52 lys2-801 ade2-101 trp1Δ63 his3Δ200 leu2Δ1 CSE4-13Myc::LEU2 pat1Δ::URA3*

Proteins were tagged at the C terminus with GFP, CFP or RFP through use of PCR cassettes unless otherwise noted.

References

1. Borland, D., and Taylor, M.R., 2nd (2007). Rainbow color map (still) considered harmful. IEEE Comput Graph Appl *27*, 14-17.
2. Stephens, A.D., Haggerty, R.A., Vasquez, P.A., Vicci, L., Snider, C.E., Shi, F., Quammen, C., Mullins, C., Haase, J., Taylor, R.M., 2nd, et al. (2013). Pericentric chromatin loops function as a nonlinear spring in mitotic force balance. J Cell Biol *200*, 757-772.

3. Quammen, C.W., Richardson, A.C., Haase, J., Harrison, B.D., Taylor, R.M., and Bloom, K.S. (2008). FluoroSim: A Visual Problem-Solving Environment for Fluorescence Microscopy. Eurographics Workshop Vis Comput Biomed *2008*, 151-158.
4. Gardner, M.K., Sprague, B.L., Pearson, C.G., Cosgrove, B.D., Bicek, A.D., Bloom, K., Salmon, E.D., and Odde, D.J. (2010). Model Convolution: A Computational Approach to Digital Image Interpretation. Cell Mol Bioeng *3*, 163-170.
5. Winey, M., and Bloom, K. (2012). Mitotic spindle form and function. Genetics *190*, 1197-1224.
6. Stephens, A.D., Haggerty, R.A., Vasquez, P.A., Vicci, L., Snider, C.E., Shi, F., Quammen, C.W., Mullins, C., Haase, J., Taylor, R.M.I., et al. (2013). Pericentric Chromatin Loops Function as a Non-linear Spring in Mitotic Force Balance Journal of Cell Biology *in press*.

Supplemental Figure 1

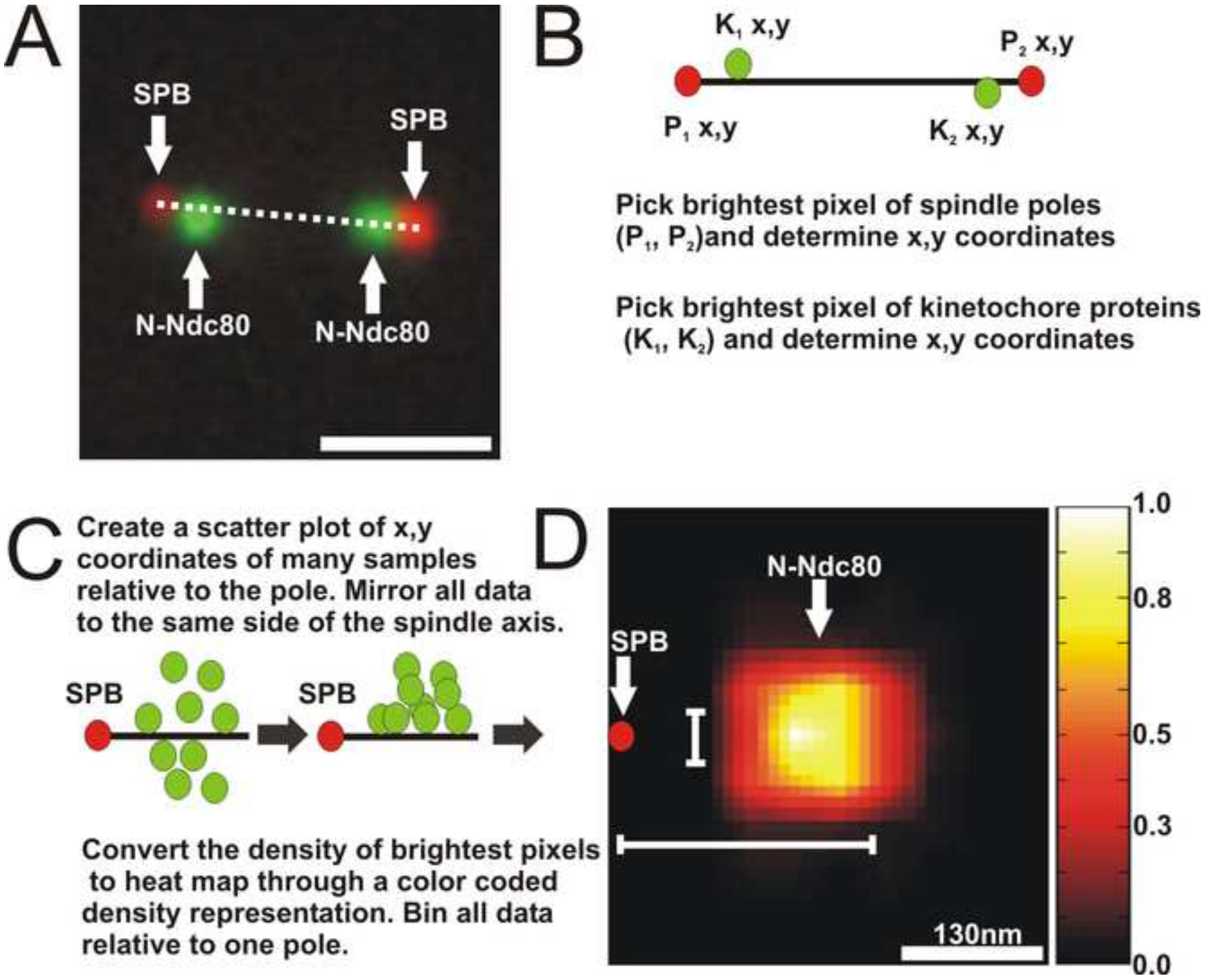

Supplemental Figure 2

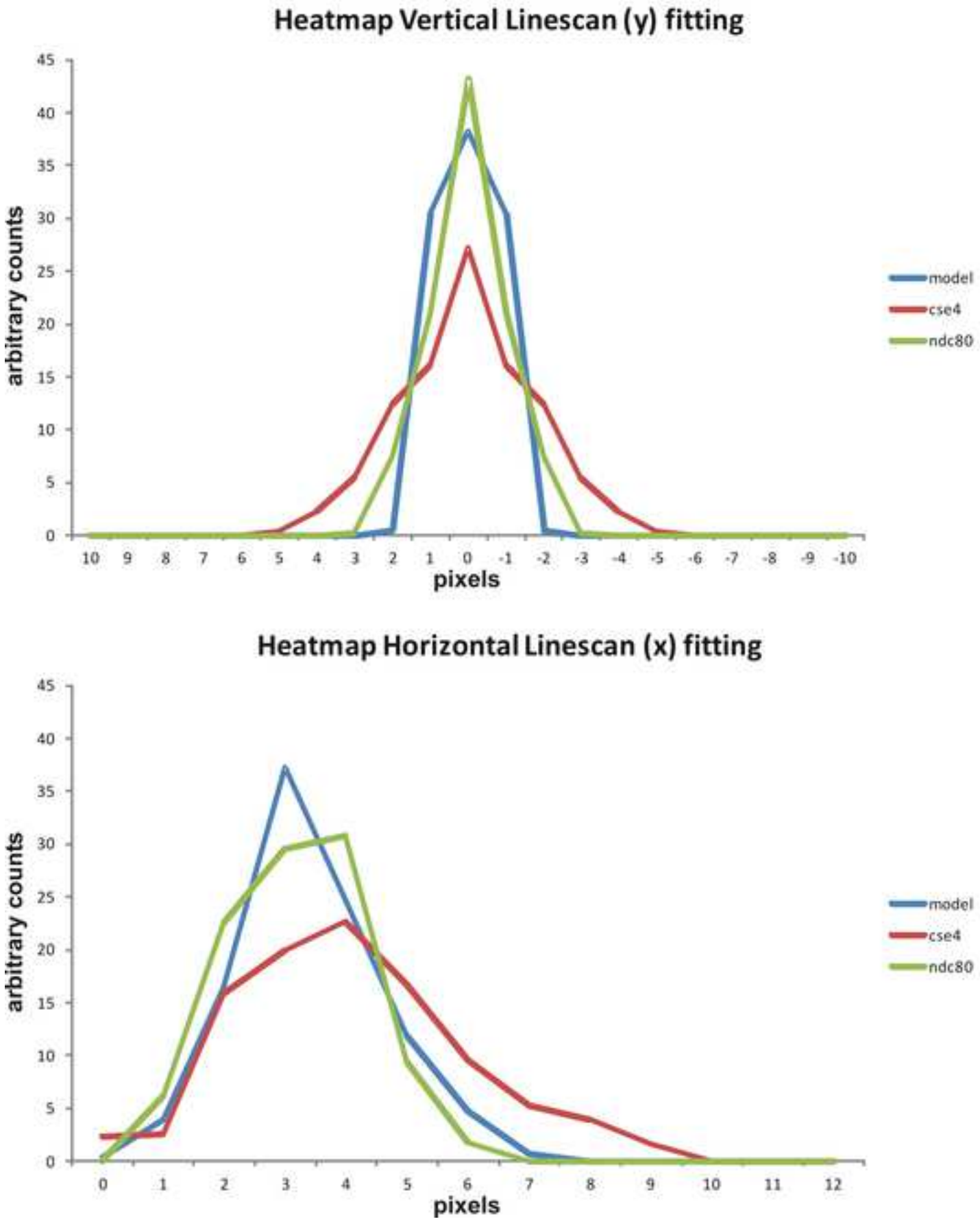

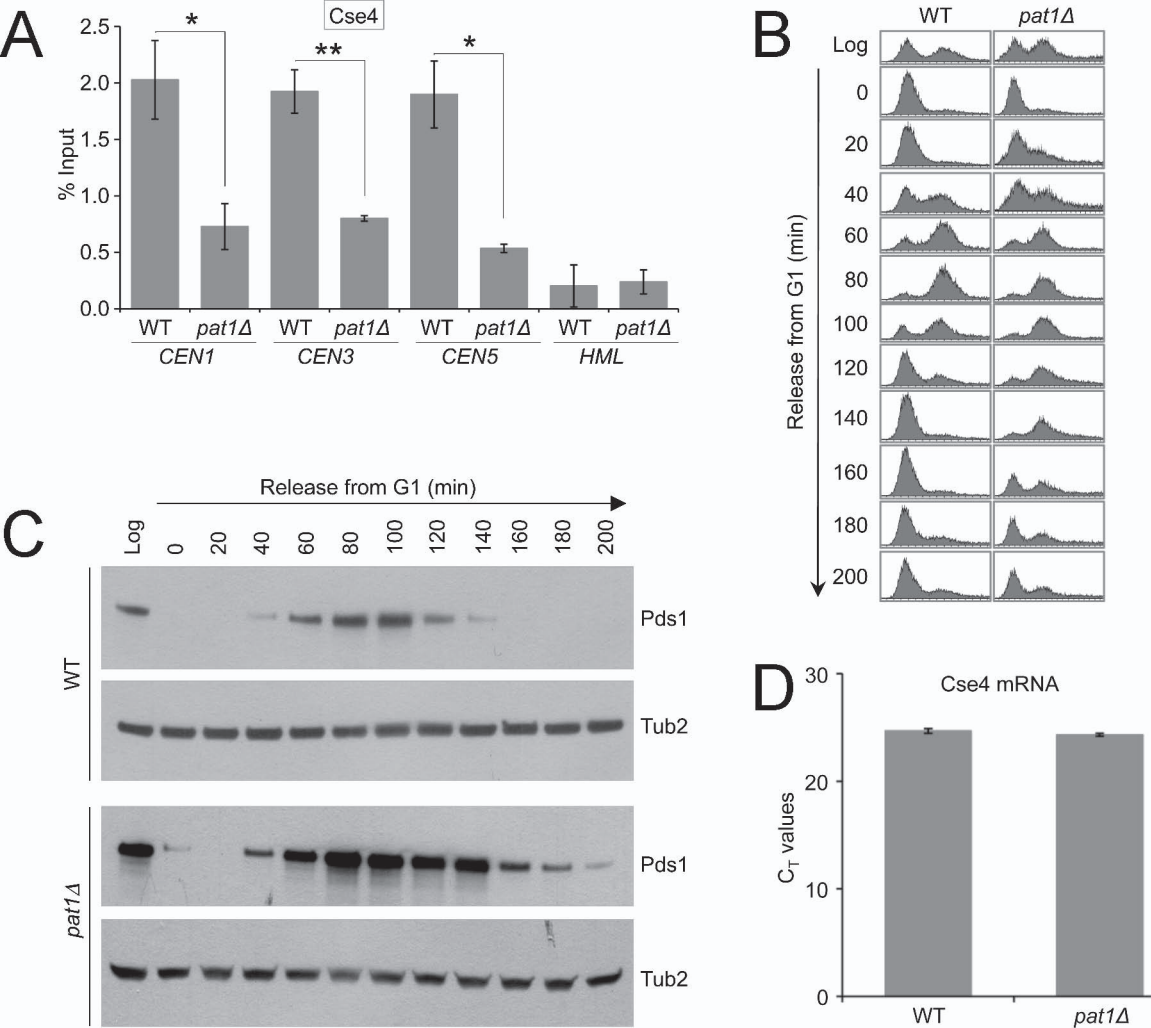
A
Cse4
% Input
2.5
2.0
1.5
1.0
0.5
0.0
*
**
*
WT
pat1Δ
CEN1
CEN3
CEN5
HML
B
WT
pat1Δ
Log
0
20
40
60
80
100
120
140
160
180
200
Release from G1 (min)
C
Release from G1 (min)
Log
0
20
40
60
80
100
120
140
160
180
200
WT
pat1Δ
Pds1
Tub2
Pds1
Tub2
D
Cse4 mRNA
C_T values
30
20
10
0
WT
pat1Δ

Supplemental Figure 4